Available online at www.sciencedirect.com
SCIENCE DIRECT®
International Journal of Thermal Sciences 44 (2005) 933–943
International Journal of Thermal Sciences
www.elsevier.com/locate/ijts

Experimental and numerical analyses of magnetic convection of paramagnetic fluid in a cube heated and cooled from opposing verticals walls

Tomasz Bednarz [a], Elzbieta Fornalik [a,b,c], Toshio Tagawa [a,b], Hiroyuki Ozoe [a,b,*], Janusz S. Szmyd [c]

[a] *Interdisciplinary Graduate School of Engineering Sciences, Kyushu University, Kasuga Koen 6-1, Kasuga 816-8580, Japan*
[b] *Institute for Materials Chemistry and Engineering, Kyushu University, Kasuga Koen 6-1, Kasuga 816-8580, Japan*
[c] *AGH University of Science and Technology, 30 Mickiewicz Ave., 30-059 Krakow, Poland*

Received 23 November 2004; received in revised form 25 March 2005; accepted 28 March 2005

Available online 12 May 2005

Abstract

The effect of a strong magnetic field on the natural convection of paramagnetic fluid in a cubical enclosure was examined. The enclosure was heated from one vertical copper wall with electric wire and cooled from the opposite wall with water pumped from a thermostating bath. The temperatures of the cooled and heated walls were measured with six thermocouples. The working fluid consisted of 80% mass glycerol aqueous solution containing 0.8 [mol·(kg of solution)$^{-1}$] of gadolinium nitrate hexahydrate to make it paramagnetic. A thermochromic liquid crystal slurry was added to the working fluid in order to visualize the temperature field in the illuminated cross-section. Numerical computations were carried out for a system corresponding to the experimental one, and computed Nusselt numbers agreed well with those obtained experimentally.

Keywords: Natural convection; Paramagnetic fluid; Magnetic field; Visualization; Numerical simulation

1. Introduction

The cubical enclosure heated from one vertical wall and cooled from an opposing wall has been employed as a benchmark system. Investigations of such geometry and conditions have mainly been related to the enhancement or suppression of heat transfer, namely, the enhancement or suppression of convection. Among a large number of published numerical and experimental works on this topic, some are close to the present work in terms of the boundary conditions [1–3], the working fluid [4] or the experimental methods [5,6].

Investigations have clearly shown that the main non-dimensional parameter related to the natural convection in the enclosure is the Rayleigh number. It determines the convective flow and it shows that the flow is controlled by the gravitational buoyancy force. In recent years, another option for flow control has appeared—the magnetic buoyancy force. The development of superconducting magnets has made the application of a magnetic field possible even on an industrial scale. Phenomena related to the magnetic field and the magnetic buoyancy force have found applications in medicine [7], chemistry [8], physics [9], engineering [10,11], and other areas.

Studies of natural convection in a cubical enclosure under a magnetic field include works by Peckover and Weiss [12] (convection of magnetic fluid in the presence of a magnetic field), Ozoe's group [13–17] (air un-

* Corresponding author. Tel.: +81 92 583 7834; fax +81 92 583 7838.
E-mail address: ozoe@cm.kyushu-u.ac.jp (H. Ozoe).

1290-0729/$ – see front matter
doi:10.1016/j.ijthermalsci.2005.03.011

Nomenclature

$\vec{b}$	magnetic induction (b_x, b_y, b_z)	T
b_0	reference magnetic induction, $= \mu_m i/l$	T
$\vec{B}$	dimensionless magnetic induction, $\vec{b}/b_0 = (B_x, B_y, B_z)$	
C	dimensionless momentum parameter for paramagnetic fluid, $= 1 + 1/(\beta\theta_0)$	
g	gravitational acceleration	$\mathrm{m\cdot s^{-2}}$
i	electric current in a coil	A
l	length of a cubical enclosure	m
Nu	Nusselt number, $= Q_{\mathrm{net\_conv}}/Q_{\mathrm{net\_cond}}$	
p	pressure	Pa
p_0	reference pressure without convection, $= \rho_0\alpha^2/l^2$	Pa
P	dimensionless pressure, $= p/p_0$	
Pr	Prandtl number, $= \nu/\alpha$	
Q_{cond}	conduction heat flux	W
Q_{conv}	convection heat flux	W
Q_{loss}	heat loss	W
$Q_{\mathrm{net\_cond}}$	net conduction heat flux, $= Q_{\mathrm{cond}} - Q_{\mathrm{loss}}$	W
$Q_{\mathrm{net\_conv}}$	net convection heat flux, $= Q_{\mathrm{conv}} - Q_{\mathrm{loss}}$	W
$Q_{\mathrm{theor\_cond}}$	theoretical conduction heat flux, $= l\lambda(\theta_{\mathrm{hot}} - \theta_{\mathrm{cold}})$	W
Q_{total}	heater power supply	W
$\vec{r}$	position vector	m
$\vec{R}$	dimensionless position vector, $= \vec{r}/l$	
Ra	Rayleigh number based on the temperature difference, $= g\beta(\theta_{\mathrm{hot}} - \theta_{\mathrm{cold}})l^3/(\alpha\nu)$	
Ra^*	modified Rayleigh number based on the heat flux, $= g\beta l^2 Q_{\mathrm{net\_conv}}/(\alpha\nu\lambda)$	
$d\vec{s}$	tangential element of a coil	m
$d\vec{S}$	dimensionless tangential element of a coil, $= d\vec{s}/l$	
t	time	s
t_0	reference time, $= l^2/\alpha$	s
T	dimensionless temperature, $= (\theta - \theta_0)/(\theta_{\mathrm{hot}} - \theta_{\mathrm{cold}})$	
$\vec{u}$	velocity vector (u, v, w)	$\mathrm{m\cdot s^{-1}}$
u_0	reference velocity, $= \alpha/l$	$\mathrm{m\cdot s^{-1}}$
$\vec{U}$	dimensionless velocity vector, $= \vec{u}/u_0 = (U, V, W)$	
x_0, y_0, z_0	reference lengths, $= l$	m
Xc	non-dimensional distance between center of the cube and center of the solenoid	

Operators

$\vec{\nabla}$	$(\partial/\partial X, \partial/\partial Y, \partial/\partial Z)$ or $(\partial/\partial x, \partial/\partial y, \partial/\partial z)$	$\mathrm{1\cdot m^{-1}}$
$D/D\tau$	$(\partial/\partial\tau + U\partial/\partial X + V\partial/\partial Y + W\partial/\partial Z)$	
D/Dt	$(\partial/\partial t + u\partial/\partial x + v\partial/\partial y + w\partial/\partial z)$	$\mathrm{1\cdot s^{-1}}$
∇^2	$\partial^2/\partial X^2 + \partial^2/\partial Y^2 + \partial^2/\partial Z^2$ or $\partial^2/\partial x^2 + \partial^2/\partial y^2 + \partial^2/\partial z^2$	$\mathrm{1\cdot m^{-2}}$

Greek symbols

α	thermal diffusivity	$\mathrm{m^2\cdot s^{-1}}$
β	thermal expansion coefficient	$\mathrm{K^{-1}}$
γ	dimensionless gamma parameter, $= \chi b_0^2/(\mu_m g l)$	
μ	viscosity	Pa·s
λ	thermal conductivity	$\mathrm{W\cdot m^{-1}\cdot K^{-1}}$
μ_m	magnetic permeability	$\mathrm{H\cdot m^{-1}}$
ν	kinematic viscosity, $= \mu/\rho_0$	$\mathrm{m^2\cdot s^{-1}}$
θ	temperature	K
θ_0	reference temperature	K
θ_{cold}	temperature of the cooled wall	K
θ_{hot}	temperature of the heated wall	K
ρ	density	$\mathrm{kg\cdot m^{-3}}$
ρ_0	reference density at temperature θ_0	$\mathrm{kg\cdot m^{-3}}$
τ	dimensionless time, $= t/t_0$	
χ	mass magnetic susceptibility	$\mathrm{m^3\cdot kg^{-1}}$
χ_m	volumetric magnetic susceptibility, $= \chi \cdot \rho$	

der a strong magnetic field) and Wang and Wakayama [18] (inhomogeneous magnetic fields and diamagnetic fluids).

Numerical analysis of non-conducting fluid has mainly involved air as a paramagnetic fluid in cubical enclosures with various configurations. Bednarz et al. [19,20] reported numerical analysis of the effect of orientation of a magnetic coil on the convection of air in a cubical enclosure. In the present work, the magnetic convection of glycerol aqueous solution with gadolinium nitrate hexahydrate was analyzed experimentally. The results were compared with those of three-dimensional numerical simulation of the same phenomenon. The computations for the corresponding configuration of the magnet are presented.

2. Experimental apparatus

The experimental setup is presented in Fig. 1. It consisted of an experimental apparatus placed in the bore of a superconducting magnet, a heater control system, a constant temperature bath and a data acquisition system connected to a personal computer. The experimental apparatus is shown schematically in Fig. 2. The Plexiglas cubical enclosure of 0.032 [m] size was heated (with constant heat flux) from one vertical wall and isothermally cooled from the opposite one, while the four remaining walls were insulated. A rubber-covered nichrome wire was used as a heater and connected to a DC power supply (Kikusui PAK 60-12A) as shown in Fig. 1. The heating power was monitored with multimeters (Keithley 2000). Water was pumped from a thermostating

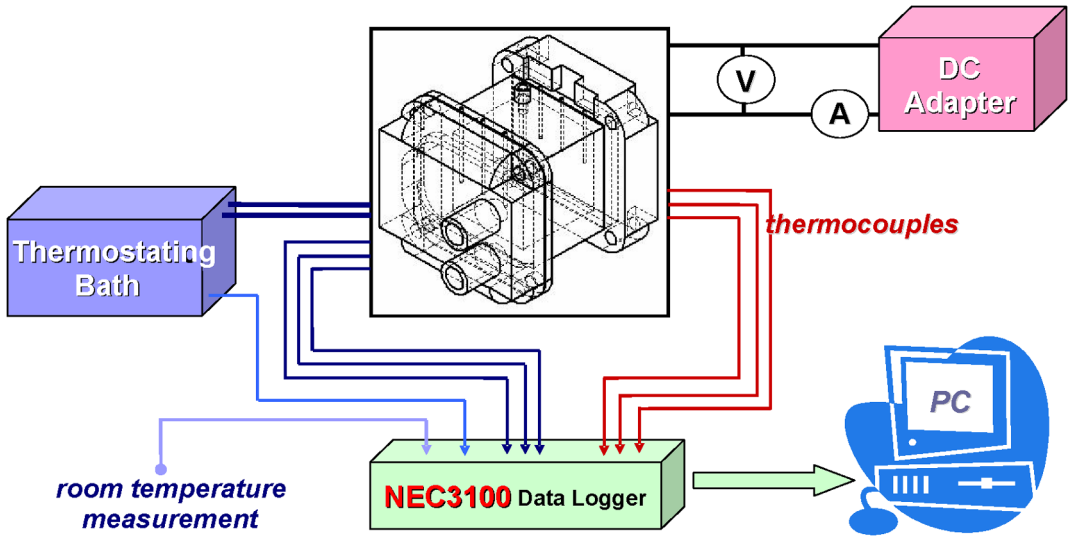

Fig. 1. Experimental setup.

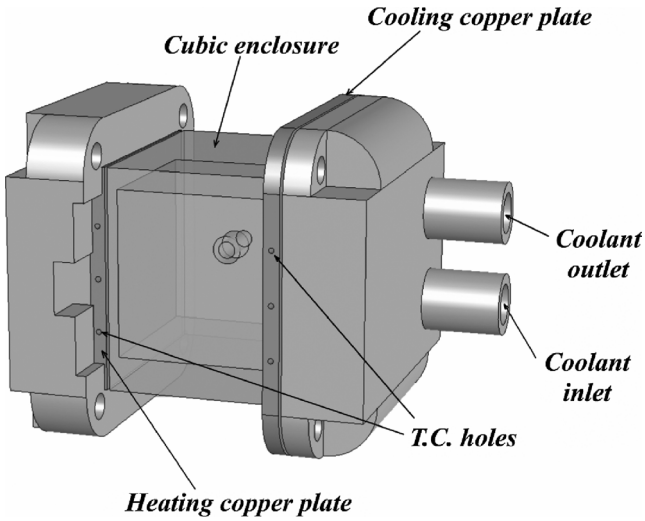

Fig. 2. Schematical view of the experimental apparatus.

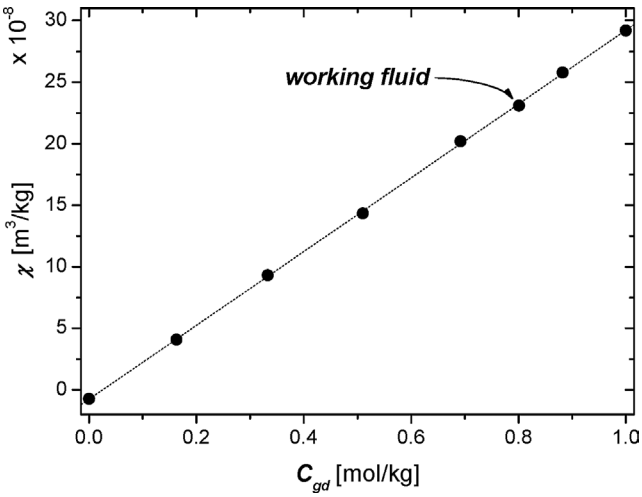

Fig. 3. Mass magnetic susceptibility versus the molar concentration of gadolinium nitrate hexahydrate in the 80% mass glycerol aqueous solution.

water bath (Fig. 1) through a small cooling chamber built in the cooling wall. The temperature of heated and cooled walls was measured with six T-type thermocouples (three in each wall). The temperatures were stored in a data logger (NEC 3100) connected to a computer (see Fig. 1). The cubical enclosure was filled with working fluid.

3. Properties of the working fluid

The working fluid was 80% mass glycerol aqueous solution. Since both glycerol and water are diamagnetic, crystals of gadolinium nitrate hexahydrate [$Gd(NO_3)_3{\cdot}6H_2O$] were dissolved in the working fluid to increase its magnetic susceptibility and make it paramagnetic. The magnetic susceptibility for various concentrations of the gadolinium nitrate hexahydrate was measured with a magnetic susceptibility balance by Evan's method (MSB Mk1). A plot of the mass magnetic susceptibility versus the molar concentration of gadolinium nitrate hexahydrate in the 80% mass glycerol aqueous solution is presented in Fig. 3.

The concentration of gadolinium nitrate hexahydrate chosen for further experiment was 0.8 [mol·(kg of solution)$^{-1}$]. This concentration corresponds to the following masses of the substrates: gadolinium nitrate hexahydrate (molar mass 0.4514 [kg·mol^{-1}]) = 0.3611 [kg], 80% mass glycerol aqueous solution = 0.6389 [kg] (mass of glycerol = 0.5111 [kg], mass of water = 0.1278 [kg]). The magnetic susceptibility of the working fluid was thereby increased from $\chi = -0.740 \times 10^{-8}$ [m^3·kg^{-1}] (for 80% mass aqueous solution of glycerol without the gadolinium nitrate hexahydrate) to $\chi = +23.094 \times 10^{-8}$ [m^3·kg^{-1}].

The density of the working fluid was measured with a pycnometer (Brand 25 ml) and was $\rho = 1463$ [kg·m^{-3}]. The viscosity was measured with an Ostwald's viscosimeter and was $\mu = 86.89 \times 10^{-3}$ [Pa·s]. The measured thermal

Table 1
Properties of the working fluid at the temperature of 298 [K]

Property	Value	Unit
α (Ref. [21])	1.01×10^{-7}	$m^2 \cdot s^{-1}$
β	0.52×10^{-3}	K^{-1}
λ (Ref. [21])	0.397	$W \cdot m^{-1} \cdot K^{-1}$
μ	86.89×10^{-3}	Pa·s
ν	5.9×10^{-5}	$m^2 \cdot s^{-1}$
ρ	1463	$kg \cdot m^{-3}$
χ	23.094×10^{-8}	$m^3 \cdot kg^{-1}$
Pr	584	–

expansion coefficient was $\beta = 0.52 \times 10^{-3}$ [K^{-1}]. Other properties were estimated from [21]. The Prandtl number $Pr = \nu/\alpha$ was estimated on the basis of measured properties and was $Pr = 584$. The properties of the working fluid are summarized in Table 1.

4. Configuration of the system

The configuration of the system is shown in Fig. 4. The superconducting magnet was set horizontally and the cubical enclosure was placed in the bore of the magnet. The center of the cube was placed at a distance of 0.070 [m] from the solenoid centre to minimize the radial component of the magnetic buoyancy force.

Experiments were carried out with magnetic induction ranging from 0 [T] to 5 [T] and an initial temperature difference ($\theta_{hot} - \theta_{cold}$) of 5.3 degrees. The initial Rayleigh number estimated from Eq. (1):

$$Ra = \frac{g\beta(\theta_{hot} - \theta_{cold})l^3}{\alpha\nu} \quad (1)$$

was $Ra = 1.49 \times 10^5$. The Rayleigh number defined in this way was employed in the numerical computations.

5. Visualization

The temperature field in the middle cross-section was visualized with thermochromic liquid crystal slurry. The liquid crystal molecule reflects definite colors depending on the temperature and viewing angle. Micro capsules containing liquid crystals are commercially available (KWN-2025, Japan Capsular Product Inc.) and there are a host of reports on this topic, for example [22]. In the present experiment, liquid crystals were mixed with the working fluid, which was then illuminated with white light generated by a projector lamp. The calibration image of the relation between temperature and color from the conduction experiment is presented in Fig. 5. Red represents the lowest temperature, and blue the highest. The temperature indicating range was from 291.2 [K] to 295.7 [K]. Color images of the temperature field were taken with a digital camera (Canon EOS

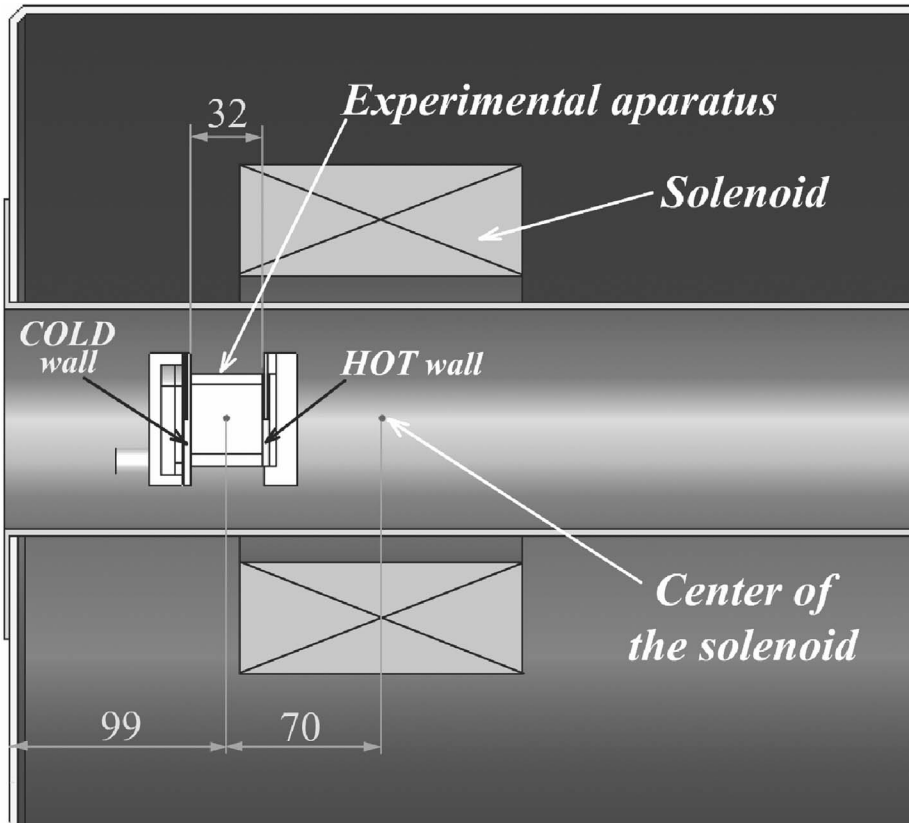

Fig. 4. Configuration of the system.

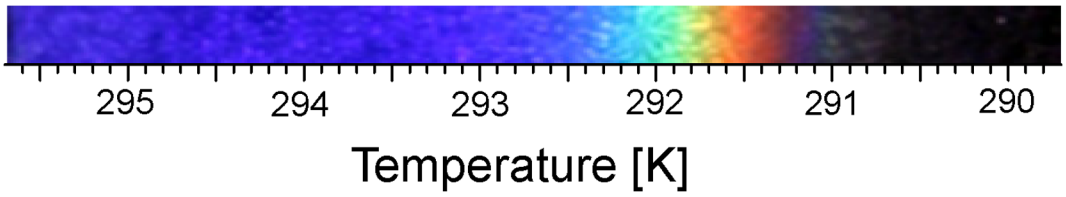

Fig. 5. Relation between color and temperature.

10D). The enclosure was removed from the magnet and set in a prepared visualization test section. This process took a few seconds and was necessary because two walls of the enclosure were non-transparent preventing visualization in the bore of the superconducting magnet. The working fluid had to be changed after a few days due to damage of the liquid crystals, which weakened their temperature response.

6. Heat transfer rate

Thermal measurements were carried out to investigate the influence of the magnetic field on the heat transfer rate. The Nusselt number is defined as follows:

$$Nu = \frac{Q_{\text{net\_conv}}}{Q_{\text{net\_cond}}} \tag{2}$$

The net convection ($Q_{\text{net\_conv}}$) and net conduction ($Q_{\text{net\_cond}}$) heat fluxes were estimated by the method of Ozoe and Churchill [23], based on the following equations:

$$Q_{\text{net\_conv}} = Q_{\text{conv}} - Q_{\text{loss}} \tag{3}$$

$$Q_{\text{net\_cond}} = Q_{\text{cond}} - Q_{\text{loss}} \tag{4}$$

It was assumed that the heat loss depends only on the temperature of heated wall and not on the heat transfer mode inside the enclosure.

As a first step in the Nusselt number estimation the conduction experiment was done. The Q_{loss} was estimated from Eq. (5):

$$Q_{\text{loss}} = Q_{\text{cond}} - Q_{\text{theor\_cond}} \tag{5}$$

where

$$Q_{\text{theor\_cond}} = l^2\lambda(\theta_{\text{hot}} - \theta_{\text{cold}})/l \tag{6}$$

was calculated from Fourier's law for the conduction area of l^2. The estimated heat loss was linearly approximated and the equation is presented below as Eq. (7)

$$Q_{\text{loss}} = 0.05739\big[(\theta_{\text{hot}} - \theta_{\text{cold}}) - 2.4574\big] \tag{7}$$

The graphical representation of net convection heat flux ($Q_{\text{net\_conv}}$) estimation is presented in Fig. 6. The slight difference in the heater power at 4 and 5 [T] is a result of removing the enclosure from the magnet. The description of method is described in Section 5.

Applying Eqs. (3), (5) and (6) to Eq. (2), the definition of the Nusselt number can be rewritten in the form

$$Nu = \frac{Q_{\text{conv}} - Q_{\text{loss}}}{l\lambda(\theta_{\text{hot}} - \theta_{\text{cold}})} \tag{8}$$

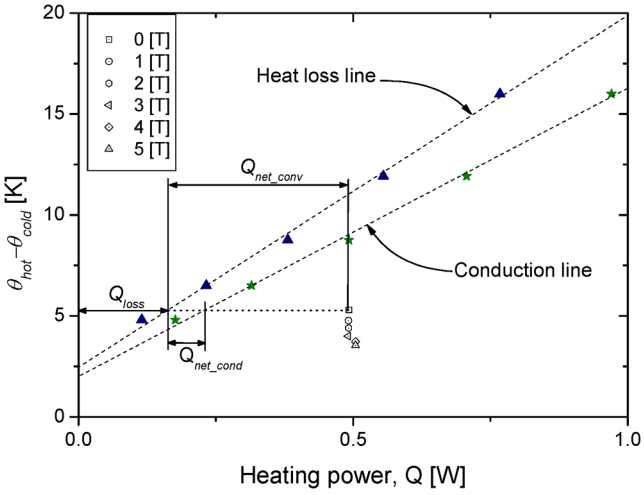

Fig. 6. Heat transfer estimation based on [23].

Table 2
Experimental conditions and results. Common parameters: $l = 0.032$ [m], $\theta_c = 18$ [°C], $Q_{\text{total}} = 0.5$ [W]

Magnetic induction b [T]	Temperature difference $\theta_{\text{hot}} - \theta_{\text{cold}}$	Rayleigh number Ra	Average Nusselt number (exp.)	Modified Rayleigh number Ra^*
0	5.3	1.49×10^5	4.889	7.3×10^5
1	4.77	1.34×10^5	5.918	7.9×10^5
2	4.4	1.23×10^5	6.801	8.4×10^5
3	4.0	1.12×10^5	7.918	8.9×10^5
4	3.73	1.05×10^5	9.102	9.6×10^5
5	3.54	0.99×10^5	9.833	9.7×10^5

The convection heat flux (Q_{conv}) is given by the product of current and voltage of the heater supply. Having the convection heat flux (Q_{conv}), the heat loss (Q_{loss}) estimated from Eq. (6) and theoretical conduction heat flux ($Q_{\text{theor\_cond}}$), it was possible to estimate the Nusselt number listed in Table 2.

The modified Rayleigh number based on the constant heat flux is as follows:

$$Ra^* = \frac{g\beta l^2 Q_{\text{net\_conv}}}{\alpha\nu\lambda} \equiv Ra \cdot Nu \tag{9}$$

This equation was applied by Poujol et al. [3]. The initial modified Rayleigh number was estimated and equal to $Ra^* = 7.3 \times 10^5$. The values of modified Rayleigh number are listed in Table 2.

7. Experimental design

The cubical enclosure was filled with the working fluid through a short pipe. After all bubbles had been removed from the interior, the outlet of the pipe was sealed. The enclosure insulated with vinyl foil and cotton-wool was placed in the bore of 5 Tesla superconducting magnet in the position described previously. The environmental temperature was kept constant. The heater power and the temperature of cooling water were set. The temperature of heated and cooled side walls were monitored continuously. After about 2 hours, when the system had reached a steady state, the temperatures and the color image were recorded. The magnetic field was then applied to the system.

The magnetic induction was increased from 1 [T] to 5 [T] by increasing the electric current to the magnetic coil in the super-conducting magnet. This usually took several minutes, because the current was changing slowly with sweep rate 0.2 [A·s^{-1}]. After each step (for example, from 0 [T] to 1 [T] or from 1 [T] to 2 [T]) the system reached the steady state after 2 hours. When the system had attained the steady state, the temperatures of the heated and cooled walls and the image of temperature field in the middle cross-section were recorded. The procedure was repeated up to the magnetic induction of 5 [T].

8. Experimental results

The visualization of temperature field in the middle cross-section at the initial Rayleigh number $Ra = 1.49 \times 10^5$ ($Ra^* = 7.3 \times 10^5$) and various magnetic inductions are presented in Fig. 7. Fig. 7(a) shows the natural convection without the magnetic field, while Figs. 7(b)–(f) show the convection under the magnetic induction from 1 [T] to 5 [T] respectively. The estimated Rayleigh numbers for each value of the magnetic induction are listed in Table 2. The left-hand wall was cooled (brown and red) while the right-hand wall was heated (blue). In Fig. 7(a), the cold fluid flowed downward, and then near the hot side wall it was heated and flowed upward. The convective roll could be observed. The color images in Figs. 7(b)–(f) suggested that the convective motion was affected by the magnetic buoyancy force. The cold fluid was strongly attracted rightward toward the center of solenoid placed behind the heated wall (Fig. 2), which is clear from the domination of the red color in the enclosure. The hot fluid was repelled leftward. The convective flow was enhanced by the increasing magnetic induction. The hot wall temperature decreased due to the enhanced convection with the constant electric heating. The Rayleigh number decreased due to the decreased temperature difference between the hot and cold walls.

9. Computational system

Fig. 8 shows a vertical cross-section of the modeled system. The cubical enclosure was cooled from one vertical wall and heated from the opposite one. Other walls were assumed to be adiabatic. The enclosure was placed in the bore of the superconducting magnet with its center on the axis of a solenoid. The non-dimensional length of the cubical enclosure was set as 1. The center of the enclosure was placed in distance $Zc = 2.19$ from the center of the solenoid. The distance Zc was chosen to minimize the radial component of the magnetizing force. The non-dimensional size of the solenoid is shown in Fig. 8. In the present computations, the solenoid was placed horizontally, close to the right-hand hot wall. This system corresponds to the real system used in the experiment.

10. Model equations

The numerical approach is based on the model for the magnetic convection of paramagnetic fluid proposed by Tagawa et al. [17]. This model employs Curie's law, which states that the magnetic susceptibility of a paramagnetic material is inversely proportional to its absolute temperature. Therefore, the temperature difference is responsible for the magnetic buoyancy force generated in such a system in the presence of the magnetic field. The experiment was carried out with a copper plate of 3 [mm] in thickness, which assumed have almost constant temperature even with electric heating. This constant-temperature wall was employed as the hot wall in the present computations. Additionally, for every numerical case, the computations were carried out with the final temperature difference obtained in the convection experiment for the corresponding case.

In the present computations, both the magnetic and gravitational convections were considered, so the dimensionless equations were given as follows:

Continuity equation:

$$\vec{\nabla} \cdot \vec{U} = 0 \tag{10}$$

Momentum equation:

$$\frac{D\vec{U}}{D\tau} = -\vec{\nabla} P + Pr\nabla^2 \vec{U} + Ra\,Pr\,T\left[(0 \quad 0 \quad 1)^{\mathrm{T}} - \gamma \frac{C}{2}\vec{\nabla} B^2\right] \tag{11}$$

Energy equation:

$$\frac{DT}{D\tau} = \nabla^2 T \tag{12}$$

Biot–Savart's law:

$$\vec{B} = \frac{1}{4\pi} \oint_{\text{multicoil}} \frac{d\vec{S} \times \vec{R}}{\vec{R}^3} \tag{13}$$

The non-dimensional variables were defined as follows:

$$X = x/x_0, \qquad Y = y/y_0, \qquad Z = z/z_0$$
$$U = u/u_0, \qquad V = v/v_0, \qquad W = w/w_0$$

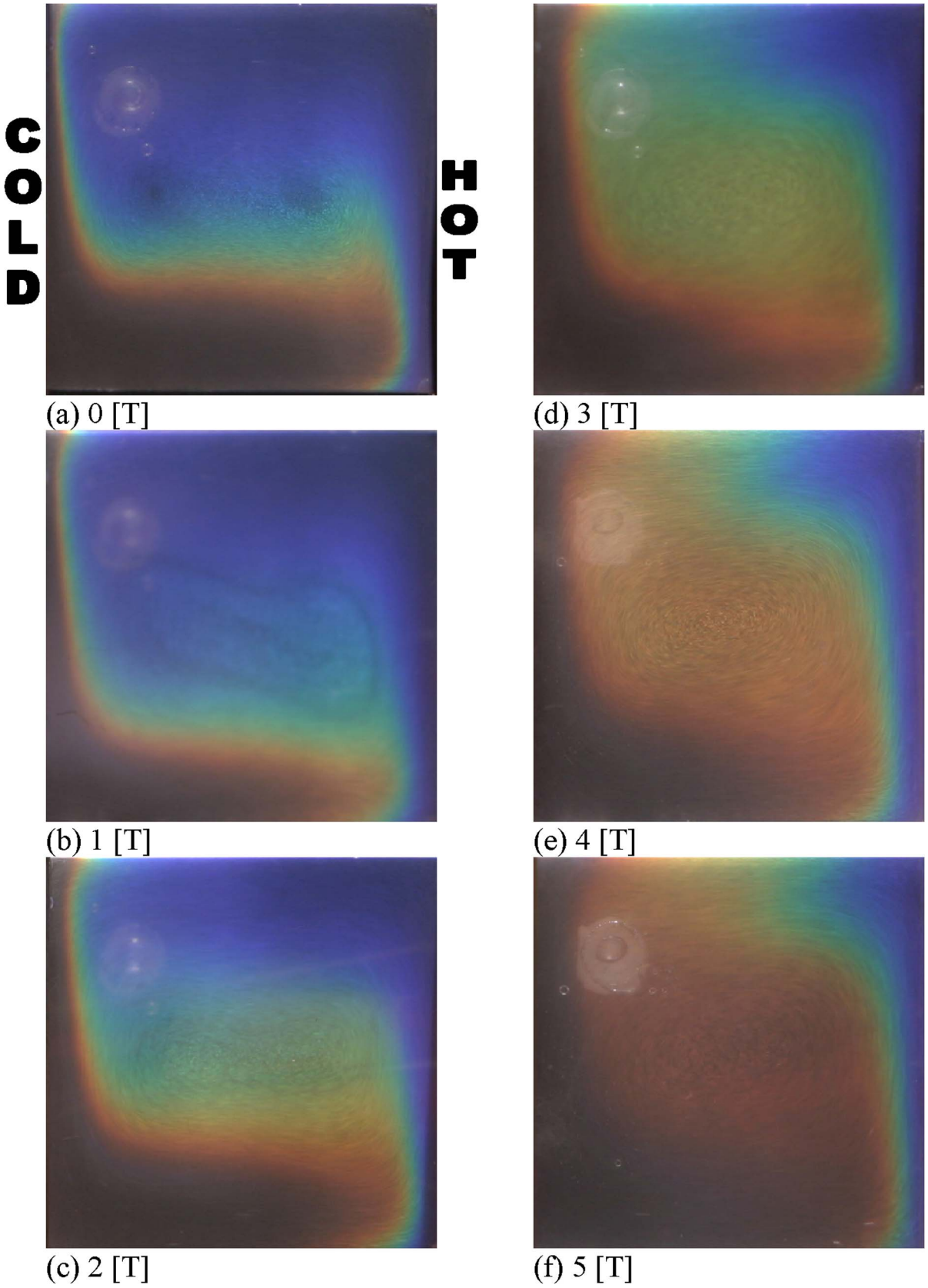

Fig. 7. Isotherms in the middle cross-section at the initial Rayleigh number $Ra = 1.49 \times 10^5$: (a) at $b = 0$ [T], $Ra = 1.49 \times 10^5$, (b) at $b = 1$ [T], $Ra = 1.34 \times 10^5$, (c) at $b = 2$ [T], $Ra = 1.23 \times 10^5$, (d) at $b = 3$ [T], $Ra = 1.12 \times 10^5$, (e) at $b = 4$ [T], $Ra = 1.05 \times 10^5$, (f) at $b = 5$ [T], $Ra = 0.99 \times 10^5$.

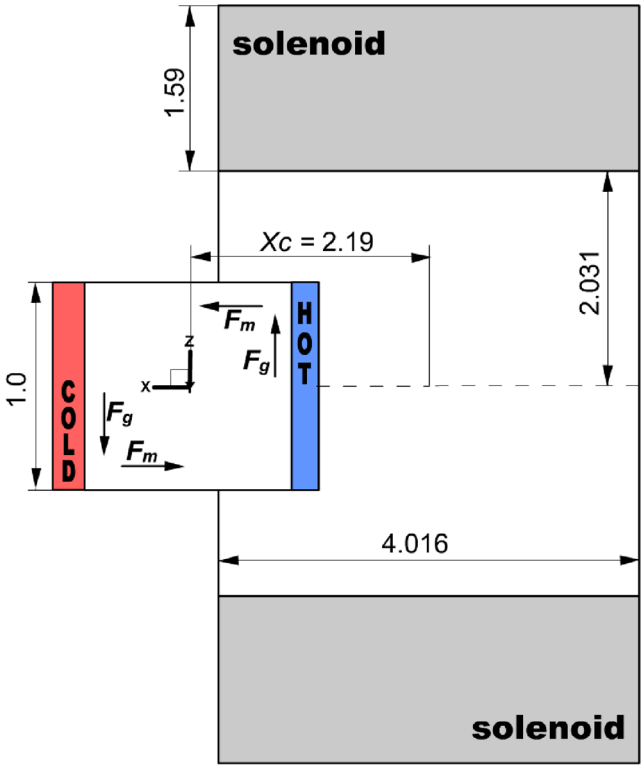

Fig. 8. Schematic view of the cross-section of the system. F_g represents the gravitational buoyancy force and F_m the magnetic buoyancy force acting on the fluid.

$$\tau = t/t_0, \qquad P = p/p_0, \qquad \vec{B} = \vec{b}/b_0$$

$$T = (\theta - \theta_0)/(\theta_{\text{hot}} - \theta_{\text{cold}}), \qquad x_0 = y_0 = z_0 = l$$

$$u_0 = v_0 = w_0 = \alpha/l, \qquad t_0 = l^2/\alpha$$

$$b_0 = \mu_m i/l, \qquad p_0 = \rho_0 \alpha^2/l^2$$

$$\theta_0 = (\theta_{\text{hot}} + \theta_{\text{cold}})/2, \qquad C = 1 + 1/(\beta\theta_0)$$

$$Pr = \nu/\alpha, \qquad Ra = g\beta(\theta_{\text{hot}} - \theta_{\text{cold}})l^3/(\alpha\nu)$$

$$\gamma = \left(\chi b_0^2\right)/(\mu_m g l)$$

The boundary conditions for this system were given as follows:

$$U = V = W = 0 \quad \text{at } X = -0.5, 0.5$$

$$Y = -0.5, 0.5$$

$$Z = -0.5, 0.5$$

$$T = 0.5 \quad \text{at } X = -0.5$$

$$T = -0.5 \quad \text{at } X = 0.5$$

$$\partial T/\partial Y = 0 \quad \text{at } Y = -0.5, 0.5$$

$$\partial T/\partial Z = 0 \quad \text{at } Z = -0.5, 0.5$$

The initial condition was a conduction state:

$$U = V = W = 0$$

$$T = -X, \quad -0.5 \leqslant X \leqslant 0.5$$

The average Nusselt number on the hot wall was defined as follows:

$$Nu = \frac{\int_{-0.5}^{0.5}\int_{-0.5}^{0.5}(\partial T_{\text{convection}}/\partial X)_{X=-0.5}\,\mathrm{d}Y\,\mathrm{d}Z}{\int_{-0.5}^{0.5}\int_{-0.5}^{0.5}(\partial T_{\text{conduction}}/\partial X)_{X=-0.5}\,\mathrm{d}Y\,\mathrm{d}Z} \tag{14}$$

The above partial differential equations were approximated by the finite difference equations. The HSMAC (**H**ighly **S**implified **M**arker **A**nd **C**ell) method was used to iterate mutually the pressure and the velocity field [24]. The number of meshes was chosen to be $40 \times 40 \times 40$. The magnetic field was computed using Biot–Savart's law for a multi-coil system to simulate the specific distribution of the magnetic field in the real system.

The Prandtl number in numerical computations was chosen to be 100. In a preliminary test computation, it was confirmed that the flow mode does not depend on the Prandtl numbers in the range of $Pr = 10$–1000. With larger Pr numbers, the iteration process took longer, up to two weeks for $Pr = 1000$. Similar comparison was done by Shyy and Chen [25].

11. Computed results

Fig. 9 shows the dimensional distribution of the magnetic induction vectors inside the bore of the superconducting magnet. This distribution was computed for the real magnet. In Fig. 9, the maximum magnetic induction is 5 [T] at the center of the solenoid at point $(r, x) = (0, 0)$. The center of the cubical enclosure was placed on the axis of the bore at a distance $x_c = 0.07$ [m] from the center of the solenoid. The $B_x(\partial B_x/\partial x)$ values computed along the axis of the bore allowed the strength of the magnetic buoyancy force acting on the fluid in the enclosure to be determined. For the numerical computations all these values were non-dimensionalized.

Table 3 summarizes the computed results for corresponding conditions of γ and Ra. The parameter C was given as follows for the experimental condition: $C = 1 + 1/(\beta\theta_0) = 1 + 1/(0.52 \times 10^{-3} \cdot 293) = 7.56$. Fig. 10 plots these results, i.e., the average Nusselt numbers versus the maximum magnetic induction, in comparison with the experimental results. The average Nusselt number at the magnetic induction of 0 [T] was around five for the experimental and numerical cases. The convective flow is present in the enclosure without the magnetic field. The heat transfer rates were increased with increasing the magnetic field. Computed Nu numbers agreed well with the corresponding experimental values. It should be mentioned that all numerical computations were carried out after the experiment in order to set all input parameters as close as possible to the real situation. The results show the enhancement of the convection with increasing strength of the magnetic field.

Fig. 11 shows the numerical results for three cases, which correspond to the experiment at the magnetic induction of 0, 1 and 2 [T]. The first column represents the force vectors $Ra\,Pr\,T[(0 \quad 0 \quad 1)^{\mathrm{T}} - \gamma\frac{C}{2}\vec{\nabla}B^2]$ shown in three horizontal

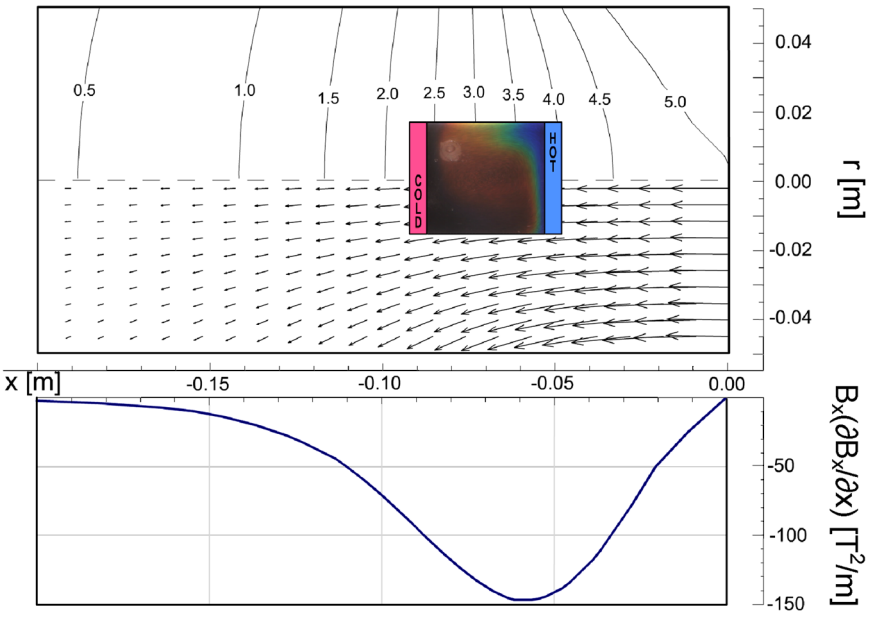

Fig. 9. Distribution of the magnetic induction inside the bore of a superconducting magnet and $B_x(\partial B_x/\partial x)$ values computed on the main axis (of the bore) at 5 [T]. Point $(r, x) = (0, 0)$ represents the center of the solenoid.

Table 3
Numerical results: Rayleigh and the average Nusselt numbers for various magnetic inductions and at $Pr = 100$, $C = 7.56$

Magnetic induction b [T]	Parameter γ	Temperature difference $\theta_{hot} - \theta_{cold}$	Rayleigh number Ra	Average Nusselt number
0	0	5.3	1.49×10^5	5.328
1	0.59	4.77	1.34×10^5	5.919
2	2.34	4.4	1.23×10^5	6.558
3	5.27	4.0	1.12×10^5	8.499
4	9.37	3.73	1.05×10^5	9.171
5	14.64	3.54	0.99×10^5	10.610

cross-sections $Z = 0.15$, 0.5 and 0.85. The second column shows the isothermal surfaces and the third one the long-time streak lines.

At the magnetic induction of 0 [T], the magnetic buoyancy force is not acting and pure gravitational natural convection can be observed. The force vectors over the hot wall are directed upward and those near the left-hand cold wall are directed downward. In the upper part relatively hot fluid prevails, and the force vectors are directed upward, in contrast to the lower part of the enclosure, where the forces are directed downward and fluid is relatively colder, as seen from the isothermal surfaces. As a result, a large roll is generated, as is seen from the long-time streak lines. The hot fluid first flows along the right-hand heated wall and later along the top ceiling toward the left-hand cold wall. Colder fluid flows downward along the cold wall and finally along the bottom adiabatic wall toward the hot wall. The average Nusselt number computed for this case was 5.328.

When the magnetic field is applied, the total force acting on the fluid is a superposition of two forces: the gravitational buoyancy force and magnetic buoyancy force. Directions of

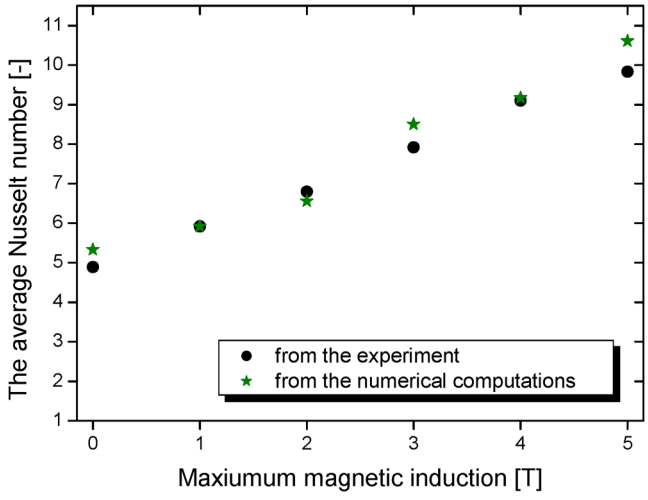

Fig. 10. Average Nusselt numbers obtained from the experiment and numerical computations. The conditions are listed in Tables 2 and 3.

these forces are shown in Fig. 8. The magnetic buoyancy force acts almost horizontally: the cube is placed where radial component of this force is minimal. In Fig. 11(b), at the magnetic induction of 1 [T], when the magnetic buoyancy force is weaker than the gravitational buoyancy force, the total force is directed askew. For stronger magnetic field, the total force is acting more horizontally as seen in Fig. 11(c) at the magnetic induction of 2 [T]. According to Curie's law, the magnetic susceptibility of paramagnetic fluid is proportional to the inverse of the absolute temperature, which is reflected in Eq. (11). That is why colder fluid is attracted toward a stronger magnetic field and hotter is repelled. In the present cases, although the direction of the flow seen from the long-time streak lines look to be similar to the case at

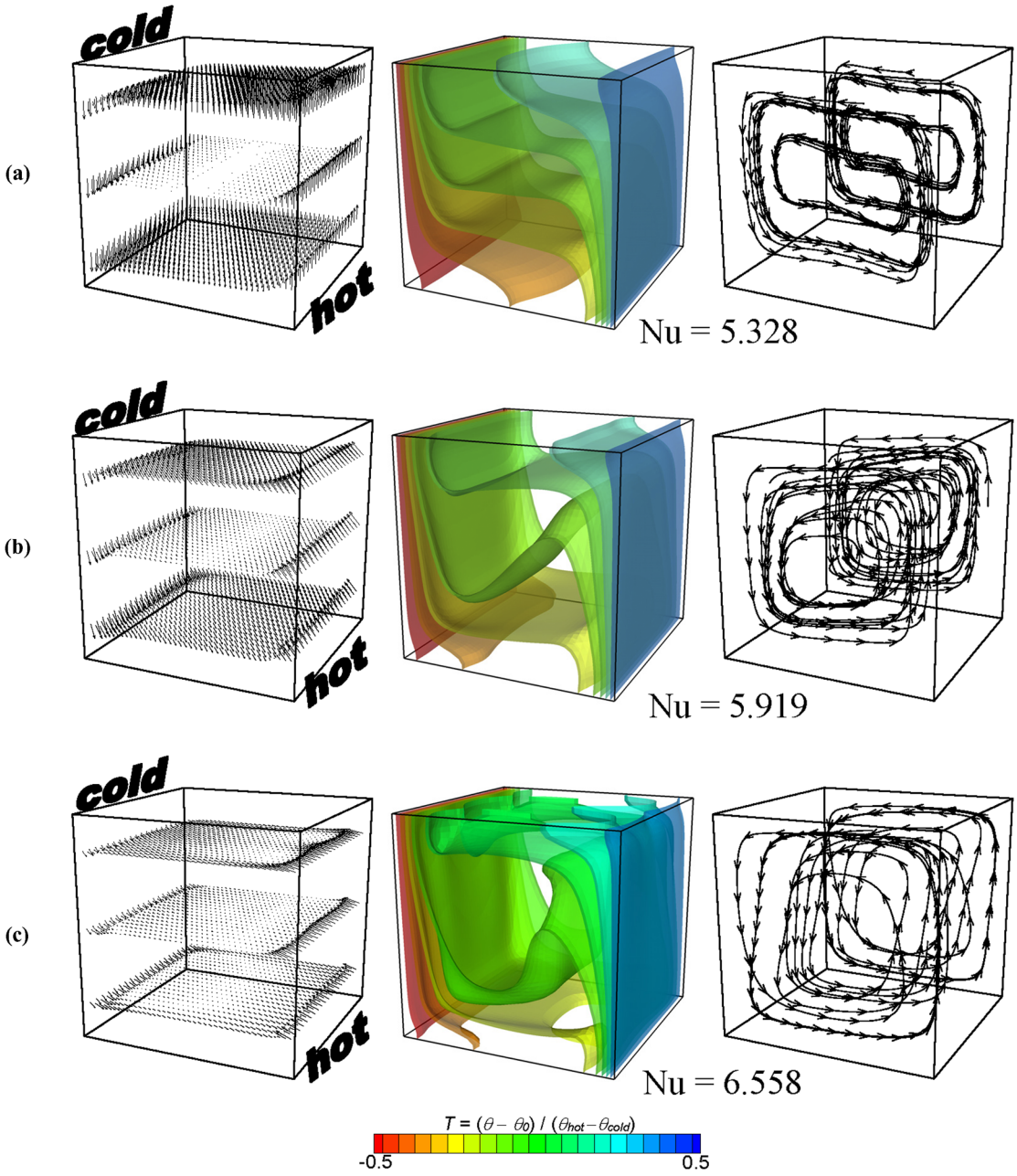

Fig. 11. Numerical results (total force vectors, isothermal surfaces and long-time streak lines) for corresponding cases with the experiment at $Pr = 100$, $C = 7.56$ and: (a) $Ra = 1.49 \times 10^5$, $\gamma = 0$; (b) $Ra = 1.34 \times 10^5$, $\gamma = 0.59$; (c) $Ra = 1.23 \times 10^5$, $\gamma = 2.34$.

0 [T], the flow and the heat transfer rate are enhanced by the magnetic buoyancy force. Temperature distribution is also affected extensively by the magnetic field.

12. Conclusions

Paramagnetic fluid convection under a strong magnetic field in a cubical enclosure was examined experimentally and by numerical analysis. The cubical enclosure was placed horizontally with the heated wall close to the magnetic coil. The experiment was carried out for various magnetic inductions. The convection motion and the heat transfer rates were intensified with increasing magnetic induction, as observed by colour visualization of isotherms and heat flux measurement.

Three-dimensional numerical computations were carried out for the system with the conditions corresponding to the experimental ones. The heat transfer rate was enhanced by the magnetic field. The average computed Nusselt numbers agreed with the results obtained in the experiment. This agreement verified the utility of the numerical code for the study of convection phenomena in a magnetic field.

Acknowledgement

This research was supported in part by European Commission (project Dev-CPPS, FP6-002968).

References

[1] T. Fusegi, J.M. Hyun, K. Kuwahara, A numerical study of 3D natural convection in a cube: effects of the horizontal thermal boundary conditions, Fluid Dynamics Res. 8 (1991) 221–230.
[2] J.M. Hyun, J.W. Lee, Numerical solutions for transient natural convection in a square cavity with different sidewall temperatures, Internat. J. Heat Fluid Flow 10 (2) (1989) 146–151.
[3] F. Poujol, J. Rojas, E. Ramos, Transient natural convection in a cavity with heat input and constant temperature wall on opposite sides, Internat. J. Heat Fluid Flow 14 (4) (1993) 357–365.
[4] C.G. Jeevaraj, J.C. Patterson, Experimental study of transient natural convection of glycerol–water mixtures in a side heated cavity, Internat. J. Heat Mass Transfer 35 (6) (1992) 1573–1587.
[5] W.J. Hiller, S. Koch, T.A. Kowalewski, Three-dimensional structures in laminar natural convection in a cubic enclosure, Experimental Thermal Fluid Sci. 2 (1989) 34–44.
[6] W.J. Hiller, S. Koch, T.A. Kowalewski, F. Stella, Onset of natural convection in a cube, Internat. J. Heat Mass Transfer 36 (13) (1993) 3251–3263.
[7] H. Onodera, Z. Jin, S. Chida, Human body risk assessment under high magnetic field environment, in: Proceedings of the 7th Symp. on New Magneto-Science, Tsukuba, Japan, 2003, pp. 208–216.
[8] K. Honda, A. Sato, S. Nakabayashi, Magneto-taxis of nonlinear chemical reaction, in: Proceedings of the 7th Symp. on New Magneto-Science, Tsukuba, Japan, 2003, pp. 52–53.
[9] C. Uyeda, K. Tanaka, M. Sakakibara, R. Takashima, Development of a method to detect magnetic anisotropy with high sensitivity in microgravity condition, in: Proceedings of the 7th Symp. on New Magneto-Science, Tsukuba, Japan, 2003, pp. 92–95.
[10] K. Ezaki, M. Kaneda, T. Tagawa, H. Ozoe, Numerical computation for the melt convection of the model system of continuous steel casting with various magnetic fields, ISIJ Internat. 43 (2003) 907–914.
[11] N.I. Wakayama, Magnetic promotion of combustion in diffusion flames, Combust. Flame 93 (1993) 207–214.
[12] R.S. Peckover, N.O. Weiss, Convection in the presence of magnetic field, Comput. Phys. Commun. 4 (1972) 339–344.
[13] M. Kaneda, R. Noda, T. Tagawa, H. Ozoe, S.S. Lu, B. Hua, Effect of inclination on the convection of air in a cubic enclosure under both magnetic and gravitational fields with flow visualization, J. Chem. Engrg. Japan 37 (2) (2004) 338–346.
[14] M. Kaneda, T. Tagawa, H. Ozoe, Convection induced by a cusp-shaped magnetic field for air in a cube heated from above and cooled from below, J. Heat Transfer 124 (2002) 17–25.
[15] R. Noda, M. Kaneda, T. Tagawa, H. Ozoe, Enhanced heat transfer rates caused by magnetic field for natural convection of air in an inclined cubic enclosure, J. Enhanced Heat Transfer 10 (1) (2003) 159–170.
[16] R. Shigemitsu, T. Tagawa, H. Ozoe, Numerical computation for natural convection of air in a cubic enclosure under combination of magnetizing and gravitational forces, Numer. Heat Transfer A 43 (2003) 449–463.
[17] T. Tagawa, R. Shigemitsu, H. Ozoe, Magnetizing force modeled and numerically solved for natural convection of air in a cubic enclosure: Effect of the direction of the magnetic field, Internat. J. Heat Mass Transfer 45 (2002) 267–277.
[18] L.B. Wang, N.I. Wakayama, Control of natural convection in non- and low-conducting diamagnetic fluids in a cubical enclosure using inhomogeneous magnetic fields with different directions, Chem. Engrg. Sci. 57 (2002) 1867–1876.
[19] T. Bednarz, T. Tagawa, M. Kaneda, H. Ozoe, J.S. Szmyd, Magnetic and gravitational convection of air with a coil inclined around the *X* axis, Numer. Heat Transfer A 46 (2004) 99–113.
[20] T. Bednarz, T. Tagawa, M. Kaneda, H. Ozoe, J.S. Szmyd, Numerical study of joint magnetization and gravitational convection of air in a cubic enclosure with an inclined electric coil, Progress Comput. Fluid Dynamics 5 (3,4,5) (2005) 261–270.
[21] VDI-Wärmeatlas, VDI-Verlag, 1997.
[22] H. Ozoe, K. Toh, T. Inoue, Transition mechanism of flow modes in Czochralski convection, J. Crystal Growth 110 (1991) 472–480.
[23] H. Ozoe, S.W. Churchill, Hydrodynamic stability and natural convection in Newtonian and non-Newtonian fluids heated from below, AIChE Sympos. Ser. Heat Transfer 69 (131) (1973) 126–133.
[24] C.W. Hirt, B.D. Nichols, N. Romero, A numerical solution algorithm for transient fluid flow, Los Alamos Scientific Laboratory, LA-5822, 1975.
[25] W. Shyy, M.-H. Chen, Effect of Prandtl number on buoyancy-induced transport processes with and without solidification, Internat. J. Heat Mass Transfer 33 (1) (1990) 2565–2578.